scientific reports

Check for updates

OPEN

Spatial chemistry of citrus reveals molecules bactericidal to *Candidatus* Liberibacter asiaticus

Alexander A. Aksenov[2,8,11]✉, Alex Blacutt[3], Nichole Ginnan[3,12], Philippe E. Rolshausen[10], Alexey V. Melnik[1,2,8], Lotfi Ali[1], Emily C. Gentry[1,13], Manikandan Ramasamy[4], Cristal Zuniga[6,14], Karsten Zengler[5,6,7], Kranthi K. Mandadi[4,9], Pieter C. Dorrestein[2,7] & M. Caroline Roper[3]

Huanglongbing (HLB), associated with the psyllid-vectored phloem-limited bacterium, *Candidatus* Liberibacter asiaticus *(C*Las), is a disease threat to all citrus production worldwide. Currently, there are no sustainable curative or prophylactic treatments available. In this study, we utilized mass spectrometry (MS)-based metabolomics in combination with 3D molecular mapping to visualize complex chemistries within plant tissues to explore how these chemistries change in vivo in HLB-infected trees. We demonstrate how spatial information from molecular maps of branches and single leaves yields insight into the biology not accessible otherwise. In particular, we found evidence that flavonoid biosynthesis is disrupted in HLB-infected trees, and an increase in the polyamine, feruloylputrescine, is highly correlated with an increase in disease severity. Based on mechanistic details revealed by these molecular maps, followed by metabolic modeling, we formulated and tested the hypothesis that *C*Las infection either directly or indirectly converts the precursor compound, ferulic acid, to feruloylputrescine to suppress the antimicrobial effects of ferulic acid and biosynthetically downstream flavonoids. Using in vitro bioassays, we demonstrated that ferulic acid and bioflavonoids are indeed highly bactericidal to *C*Las, with the activity on par with a reference antibiotic, oxytetracycline, recently approved for HLB management. We propose these compounds should be evaluated as therapeutics alternatives to the antibiotics for HLB treatment. Overall, the utilized 3D metabolic mapping approach provides a promising methodological framework to identify pathogen-specific inhibitory compounds *in planta* for potential prophylactic or therapeutic applications.

Huanglongbing (HLB) is a highly destructive citrus disease exhibiting complex symptomatology. As one of the most serious plant diseases worldwide, HLB poses a major threat to US citrus production, which is primarily concentrated in Florida, California, Arizona, and Texas[1]. All commercial citrus varieties are HLB-susceptible to various degrees and HLB has been identified in 51 out of 140 countries that produce citrus[2]. HLB is caused by the bacterium *Candidatus* Liberibacter asiaticus (*C*Las) and is spread by the insect vector *Diaphorina citri*, commonly known as the Asian Citrus Psyllid (ACP). Early HLB symptoms include leaf mottling and yellow shoots, which leads to root dieback and tree death[3]. Moreover, the effect on fruit development has major downstream consequences on fresh fruit and juice quality[4]. Fruit from HLB-infected trees are small, misshapen, with irregular

[1]Department of Chemistry, University of Connecticut, Storrs, CT, USA. [2]Collaborative Mass Spectrometry Innovation Center, Skaggs School of Pharmacy & Pharmaceutical Sciences, University of California – San Diego, La Jolla, CA, USA. [3]Department of Microbiology and Plant Pathology, University of California, Riverside, CA, USA. [4]Department of Plant Pathology and Microbiology, Texas A&M AgriLife Research and Extension Center, Weslaco, TX, USA. [5]Department of Pediatrics, University of California, San Diego, La Jolla, CA, USA. [6]Department of Bioengineering, University of California, San Diego, La Jolla, CA, USA. [7]Center for Microbiome Innovation, University of California, San Diego, La Jolla, CA, USA. [8]Arome Science Inc., Farmington, CT, USA. [9]Institute for Advancing Health Through Agriculture, Texas A&M AgriLife, College Station, TX, USA. [10]Department of Botany and Plant Sciences, University of California, Riverside, CA, USA. [11]Present address: Department of Chemistry, University of Connecticut, Storrs, CT, USA. [12]Present address: One Health Microbiome Center, Huck Institutes of the Life Sciences, Pennsylvania State University, University Park, PA, USA. [13]Present address: Department of Chemistry, Virginia Tech, Blacksburg, VA, USA. [14]Present address: Department of Biology, San Diego State University, San Diego, CA, USA. ✉email: aaksenov@uconn.edu

maturation patterns that yield unpalatable flavor profiles. The disease has a long asymptomatic stage, making early detection and management particularly challenging[4,5].

The ACP, first reported in Florida in 1998, caused rapid regional HLB outbreaks by 2005, resulting in endemic establishment and billions of dollars in damages in industry[5,1]. ACP has since spread east to west across the US citrus belt, and HLB is now detected in thousands of Californian urban citrus plants, threatening commercial groves[6]. This rapid spread of HLB follows a consistent pattern: once the ACP vector establishes itself in a new area, HLB typically appears soon after. Disease management has mainly focused on insect vector control with repeated sprays of synthetic insecticides[7], and no sustainable bacterium-targeting HLB interventions yet exist. The uneven distribution of *C*Las within infected trees further complicates reliable detection using PCR and assessment of chemical and biological perturbations caused by the bacterium[8]. While HLB-specific microbial and molecular biomarkers[9], and HLB-induced proteome changes have been identified[10,11], these advances have yet to translate into effective disease management strategies.

*C*Las is a phloem limited bacterium, that can not be axenically cultured[8]. The phloem is a high pressure vascular tissue that transports photosynthates (metabolic products) and sugars throughout the plant. These features of the pathosystem make it particularly difficult to study and manage. Currently, oxytetracycline antibiotic trunk injection is the primary approach to reduce and control *C*Las[12–14]. However, antibiotic deployment is economically unsustainable for growers and imposes risk to human and environmental health by potentially increasing antimicrobial resistance in bacterial populations. A "precautionary tale"—widespread antibiotic administration has led to the rapid emergence of resistant *Candidatus* Liberibacter asiaticus strains in China[15]. Thus, alternative bactericidal agents need to be explored for viable and sustainable approaches to *C*Las control.

Metabolomics, both nuclear magnetic resonance (NMR) and mass spectrometry (MS)-based, gives valuable insights into molecular distributions, including those underlying pathogenesis, and thus may provide leads on potential therapeutic molecules. These techniques have repeatedly demonstrated their value in providing important insights into pathogenesis and the mechanistic details of underlying biology[16,17]. Past investigations employing NMR and MS established associations between *C*Las infection, such as terpenoid/sugar disruption underlying symptomatic flavor decline[18]. However, uneven HLB distribution hinders generalizing systemic changes[19,20]. As symptoms manifest locally, pinpointing locally perturbed metabolites is essential to understand the disease and propose targeted therapies.

Recent advances in metabolomics enable exploring spatial chemical distributions[21–24]. This includes mass spectral molecular networking, which supports annotation propagation within a network of compounds clustered based on their structural similarities[25]. This method can capture metabolomic transformations and cluster related compounds, partially addressing the challenge of sparse annotation due to limited compound libraries. We hypothesized that detailed infection mapping would expedite discovery of compounds active against *C*Las *in planta*, to provide candidates for novel HLB therapeutics. In this work, we visualized the HLB effect on the metabolome of citrus plants using 2D and 3D molecular maps to gain pathological insights, illuminating possible bacterium-mediated host metabolite exploitation. While we focused on citrus, this approach, in principle, should be generally applicable to a wide range of plant-pathogen systems.

Results

Metabolome shifts in field and greenhouse trees with HLB

We carried out an untargeted metabolomics analysis of citrus tree tissues across a spectrum of disease severity collected from seven HLB-infected Florida orchards, where the disease is endemic. Tissues throughout the citrus tree: stems, roots, and leaves were collected and analyzed. Because of the complex metabolome of citrus trees across different tissues, we used molecular networking[25,26] to map and explore the detected chemistries. The resulting network grouped molecules that fragmented in a similar fashion, thus capturing their structural similarity and aiding in understanding the chemical distributions[26,27]. The network of the detected metabolome across grove trees is shown in Fig. 1a,b. The metabolome varied as HLB progressed (Fig. 1c), with molecules associated with disease severity forming distinct clusters in the network. This suggests that metabolic disruption in HLB progresses not through individual molecular changes, but shifts across entire biochemical families. Clusters of compounds—dilinolenins, fatty amides like octadecenamide, glycerophosphocholines, terpenoids, and, prominently, flavonoids—showed changes linked to symptom severity across tissues. To control for confounding factors such as length of infection, local conditions etc., samples were also collected from a controlled greenhouse environment, including infected and uninfected healthy trees (confirmed using qPCR). Metabolome differences related to HLB symptomatology were much more pronounced in greenhouse samples as compared to field samples, even though symptoms were significantly less pronounced. The most discerning diagnostic markers, identified via partial least squares discriminant analysis (PLSDA) and Random Forest, were found to be various flavonoids. This implicates the flavonoid pathway as the main metabolomic "barometer" of infection[19,28–33].

3D metabolome mapping

To explore the spatial patterns in distribution of metabolites, molecular maps were generated using the *'ili* tool[21]. We further elucidated these patterns for HLB-discriminating molecules. This mapping was conducted on tissues from greenhouse-reared trees of the same age and length of infection. 3D metabolome maps were rendered by collecting individual leaves along an infected branch and mapping specific metabolite concentrations, such as the flavonoid scutellarein tetramethyl ether, back to branch images (Fig. S1). This allowed for visualization of metabolite concentration along the same branch where apical leaves exhibited HLB symptoms and basal leaves are asymptomatic (Fig. S1a). Notably, the distribution of the flavonoid scutellarein tetramethyl ether may be related to leaf age rather than symptomology. Therefore, the symptom-related patterns were investigated at single-leaf resolution, where leaves are age-matched. At this scale, symptom-related patterns were noticeable to

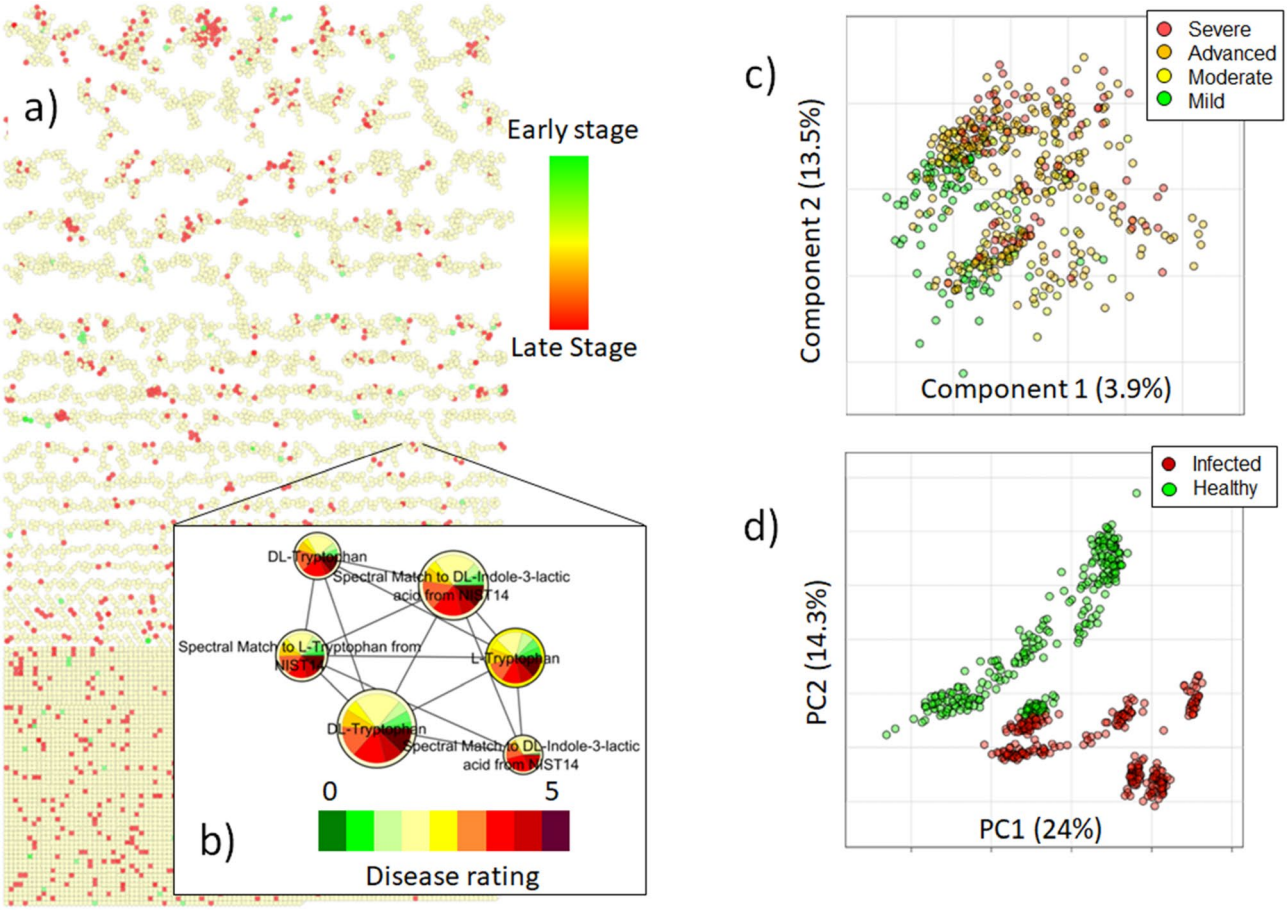

Fig. 1. Global network analysis of metabolomic shifts in HLB-infected trees. Citrus trees (leaves, stems and roots) were sampled across multiple groves in Florida. (**a**) Global network of the metabolome detected in samples collected from grove trees in Florida, which included trees exhibiting symptoms across a range of disease severity (1—appears healthy to 5—severe HLB symptoms). (**b**) A close-up of a network cluster showing distributions of molecular abundances in trees with different disease ratings (higher values correspond to higher symptom severity); node size is related to total compound abundance. The compounds in the cluster were present in higher amounts when the disease was more severe. The selected example shows perturbation in amounts of tryptophan, indicative of altered metabolism, and a metabolite known to be of microbial origin, indole-3-lactic acid (ILA), a tryptophan metabolite that is known to play a role in microbe-host interactions; ILA is associated with increased disease severity. (**c**) A supervised analysis (partial least squares discriminant analysis, PLSDA) of tissues from trees in orchards across Florida showed metabolome stratification according to disease severity (Q2 0.1775). (**d**) Unsupervised analysis (principal component analysis, PCA) of tissues from greenhouse-reared trees indicated drastic differences in the metabolome of healthy and infected symptomatic tissues.

an expert, with various flavonoids sharing similar spatial propagation pattern; depleted in visibly chlorotic and mottle signatures of infection (Fig. S2). At the same time, oxidized flavonoids tended to exhibit opposite spatial patterns, suggestive of mutual interconversion (Figs. 2, S3).

Other than flavonoids, we noted feruloylputrescine, a conjugate of ferulic acid (part of the flavonoid biosynthesis pathway) and putrescine as molecules descriptive of HLB symptoms. Feruloylputrescine is preferentially accumulated in apical symptomatic leaves, exactly opposite the non-oxidized flavonoid depletion patterns (Fig. S4a). The ferulic acid abundance decreased concomitantly with putrescine conjugation, indicative of the possible conversion into feruloylputrescine (Fig. S4b). The same trends were evident on the single-leaf scale, with a clear correspondence of spatial distributions to the chlorotic spots phenotype (Fig. 3; note that in greenhouse-grown plants the visual differences may not be stark, particularly in early or mild infection). Another related phenolic acid, hydroxycinnamic acid (*p*-coumaric acid), showed a similar distribution, enriched in symptomatic areas (Figs. S5, 3C).

Metabolic modeling of *C*Las uptake rates of plant metabolites

A possible rationale for the observed spatial patterns in the metabolome (in particular, the low abundance of ferulic acid in symptomatic tissue) may be the metabolism of ferulic acid by the bacterium that would protect itself from antimicrobial activity. A supporting argument for this would be the observation that phenolic acids,

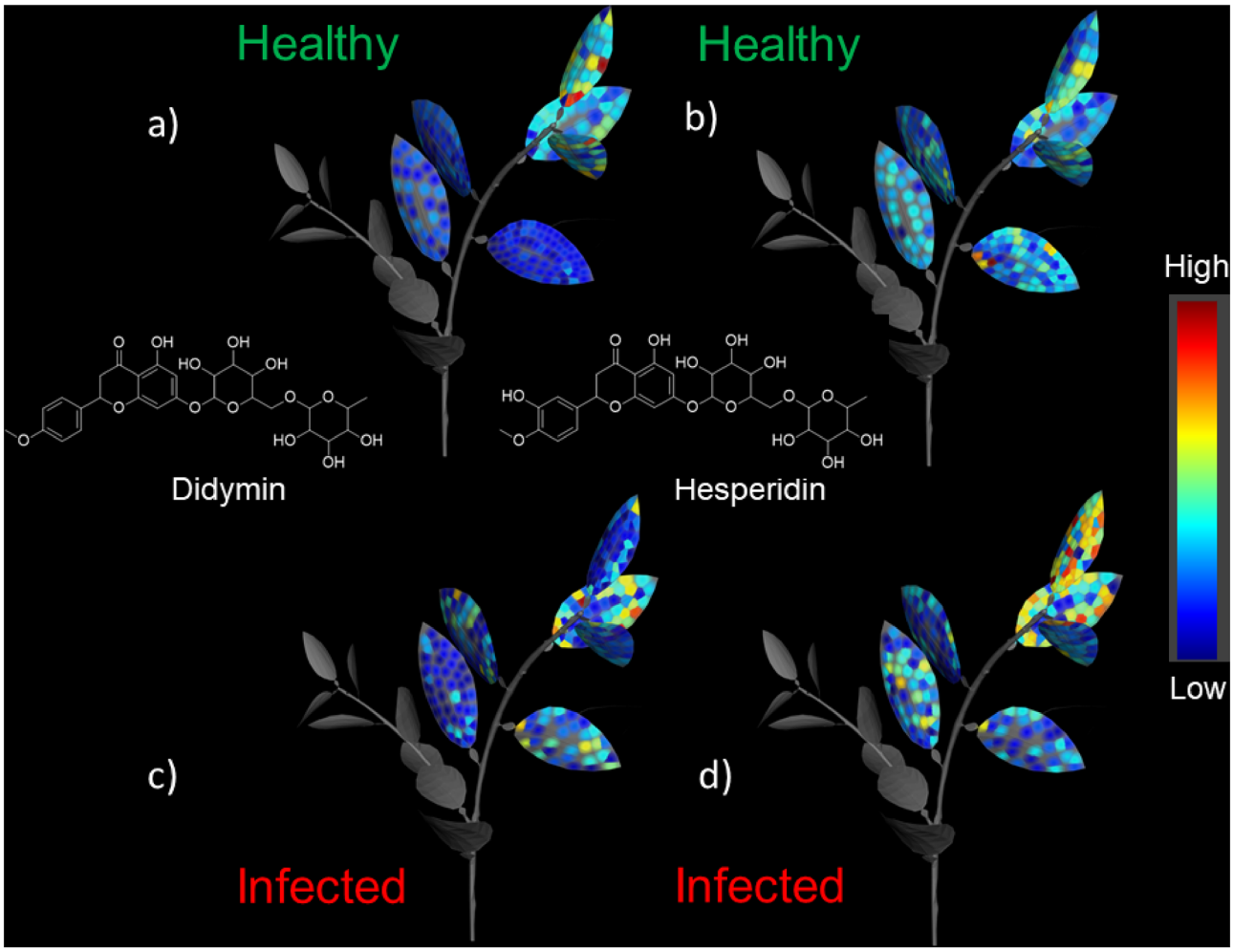

Fig. 2. 3D mapping of the distribution of the flavonoids, didymin and hesperidin in infected and healthy citrus branches: (**a**) Didymin (m/z 595.2026 (rt 208.16)), (**b**) Hesperidin m/z 611.1973 (rt 131.25)) and infected plant: (**c**) Didymin and (**d**) Hesperidin. Didymin was present at higher abundance in younger leaves of healthy plants and was depleted in the infected plant, while hesperidin increased in abundance in the infected plant and didymin was depleted, indicating possible formation of hesperidin due to oxidation of didymin.

like ferulic acid, reduce the growth rate of *C*Las, while in conjugation with putrescine, this effect is reduced due to the synthesis of feruloylputrescine. Therefore, we tested this hypothesis by conducting model simulations using the previously established genome-scale metabolic network of *C*Las[15]. We simulated uptake rates of plant metabolites by *C*Las for compounds that are part of arginine and proline metabolism, as well as those present in the biosynthesis of phenylpropanoids. The model predicted that uptake rates of ferulic acid between 1×10^{-10} and 1×10^{-8} mmol/gDW/h would be sufficient to reduce the growth rate of *C*Las up to 90%. These predictions were experimentally confirmed and putrescine uptake rates in this range did not predict a reduction of *C*Las growth. Interestingly, when these ferulic acid uptake rates (1×10^{-10} and 1×10^{-8} mmol/gDW/h) were combined with putrescine uptake rates between 1×10^{-2} and 10×10^{-1} mmol/gDW/h, the model predicted the highest *C*Las proliferation (Fig. 4).

In vitro verification of model predictions with disc assay

In order to further confirm in silico predictions, we assayed putrescine, ferulic acid, and feruloylputrescine for potential antibacterial activity using a previously developed disc diffusion assay based on *Liberibacter crescens*, a culturable surrogate of the unculturable *C*Las[34]. Metabolic modeling of the pathogen described in the "Metabolic modeling of *C*Las uptake rates of plant metabolites" section above predicted putrescine and feruloylputrescine to be mildly beneficial and ferulic acid to be inhibitory to *C*Las growth. The model predictions were consistent with the metabolites' spatial distributions in greenhouse citrus tree leaves. Disc assay results showed that putrescine and ferulic acid were indeed moderately and highly inhibitory to *L. crescens,* respectively. The conjugated metabolite, feruloylputrescine, was not inhibitory to *L. crescens* growth as predicted by our model (Fig. 3D). These in vitro results, in conjunction with the observed interconversion between ferulic acid, putrescine, and feruloylputrescine in HLB symptomatic trees, indicate that *C*Las likely directly, or through manipulation of host

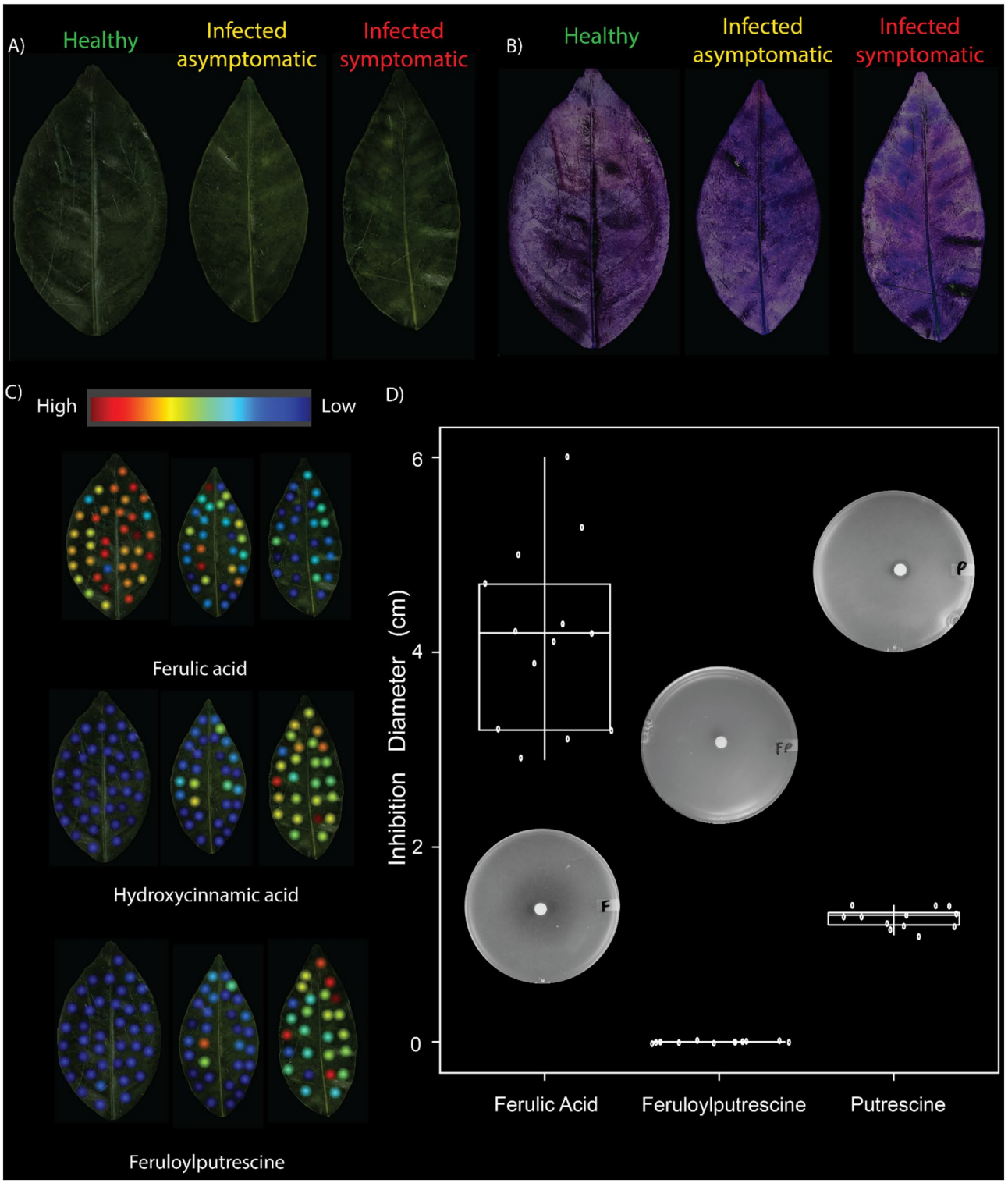

Fig. 3. 2D mapping of polyamine derivatives within single leaves. (**A**) Unmodified images of leaves with different disease severity; the symptoms are subtle, with chlorotic spots appearing as slightly lighter areas. (**B**) The leaves shown in (**A**) in a color scheme that more clearly shows chlorotic spots (chlorotic spots appear as dark shade areas). (**C**) Mapped distributions of (top to bottom): ferulic acid—H_2O (only water loss ion was observed), hydroxycinnamic acid and feruloylputrescine. 2D maps: healthy, infected asymptomatic, infected symptomatic (from left to right). The mapped symptomatic and asymptomatic leaves were sampled from two branches of a tree that was confirmed by qPCR to be infected with *C*Las ($C_t = 19.6$). Increases in hydroxycinnamic acid and feruloylputrescine were concomitant with increased disease severity, while ferulic acid exhibited the opposite trend. (**D**) Plot showing *Liberibacter crescens* (a culturable surrogate for *C*Las) growth inhibition assay, when challenged with 35 mg/mL solution by ferulic acid, feruloylputrescine or putrescine as quantified by the diameter of the zone of inhibition. Ferulic acid had a pronounced inhibition effect.

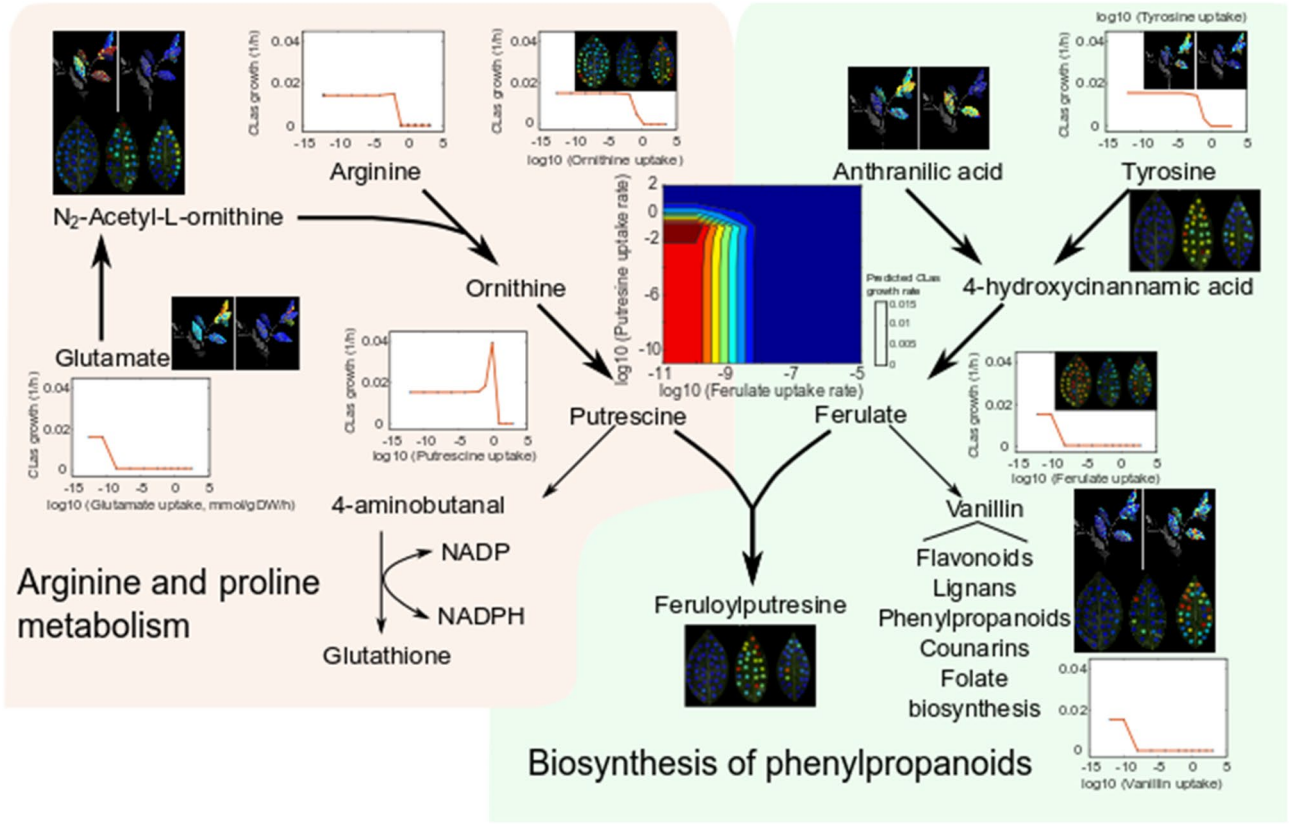

Fig. 4. Genome-scale metabolic network simulations about the effect of feruloylputrescine biosynthesis on the growth of *C*Las. Contour plot shows the predicted growth rates of *C*Las, while varying putrescine and ferulate uptake rates. Individual scatter plots show the response of *C*Las growth to changes in the individual uptake rates of metabolites of interest (mmol/gDW/h). 2D maps of leaves show from left to right: healthy, infected symptomatic, infected asymptomatic samples of citrus plants. 2D maps of plants show from left to right: healthy and infected citrus plants.

metabolic pathways, conjugate ferulic acid to putrescine producing the non-toxic feruloylputrescine, which increasing its survivability in the host.

Ex vivo verification of model predictions with *C*Las-citrus hairy root assay

To further validate the toxicity of ferulic acid and flavonoids, whose biosynthesis is disrupted due to conjugation, against the target pathogen *C*Las, we conducted a *C*Las-citrus hairy root cultures assay[35]. As a possible low-cost, accessible therapeutic intervention, we tested over-the-counter citrus peel extracts as a widely available source of native citrus bioflavonoids. *C*Las-containing hairy roots were treated with bioflavonoids and ferulic acid for 72 h (Fig. 5a). Untreated and ethanol (0.2% v/v) samples were used as negative controls. A reference antibiotic, oxytetracycline (OXY), reported as an inhibitor of Clas[14,36,37], was used as a positive control. After treatment, all tissue samples were exposed to PMAxx dye (propidium monoazide, Biotium, Fremont, CA) that allows measurement of only live *C*Las bacterial DNA, following DNA extraction and molecular diagnostics. The relative titers of *C*Las were estimated using qPCR. We found that bioflavonoids significantly inhibited *C*Las ($p \leq 0.05$) in a dose-dependent manner (125, 250, and 500 ppm), whereas ferulic acid showed inhibition at 125 and 250 ppm ($p \leq 0.05$), on par with oxytetracycline when compared to untreated controls (Fig. 5b).

Discussion

We explored HLB disease metabolome dynamics using spatial mapping, predictive modeling, in vitro, and ex vivo assays to identify endogenous citrus compounds with plant therapeutic potential. Metabolites altered by HLB symptoms were consistent among field and greenhouse trees, with flavonoids comprising the most discriminating "biomarkers", supporting previous observation[19,37–39]. The discriminant flavonoids structures did not comport to a notable trend, and molecules differing by various backbone substitutions, e.g. addition of a glycan (which increases the compound's solubility), were found to be predominantly declining in infected symptomatic tissues. This implies upstream flavonoid pathway suppression that potentially aids pathogen establishment, fitting the known antimicrobial and defense roles of these compounds. However, this information alone is insufficient to understand disease etiology[9,37,38,40]. For example, certain flavonoids were instead found to increase with HLB symptom development.

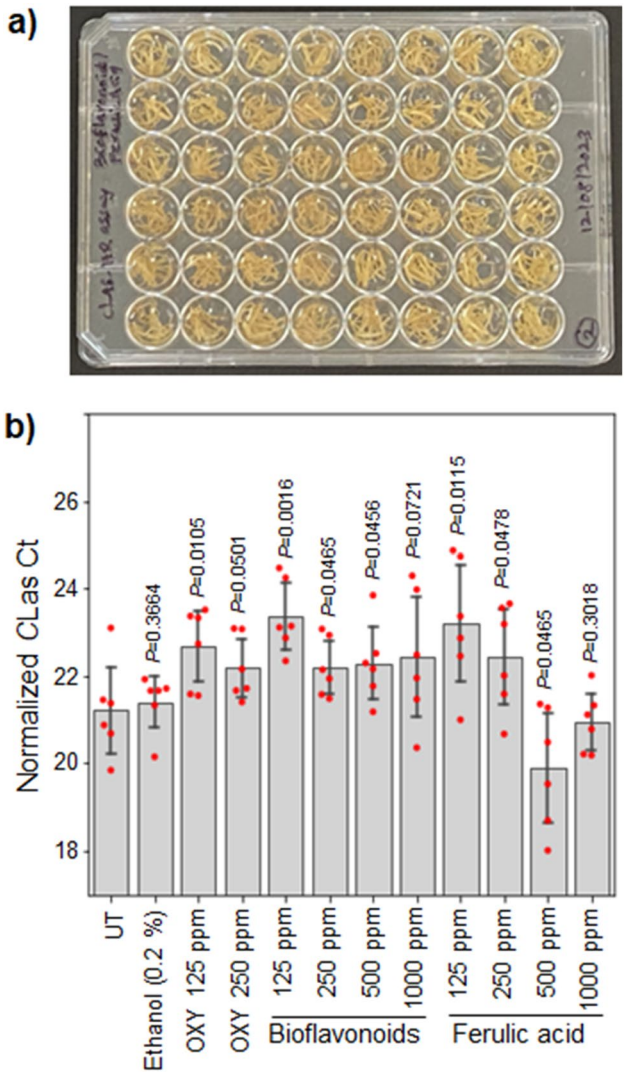

Fig. 5. Bioflavonoids and ferulic acid inhibit the growth of *Candidatus* Liberibacter asiaticus (*C*Las) in *C*Las-citrus hairy roots. (**a**) The *C*Las-citrus hairy roots were treated for 72 h with 125, 250, 500, and 1000 ppm of bioflavonoids and ferulic acid. Oxytetracycline hydrochloride (OXY)-treated hairy roots (250 and 500 ppm) were used as a positive control, and untreated (UT), ethanol (0.2%) used to dissolve the compounds was used as a negative control. Relative titers of *C*Las (**b**) were estimated after 72 h of treatment, followed by qPCR analysis. Error bars represent the standard error of the mean (n = 6), and *p* values were calculated by Student *t*-test relative to untreated samples.

Overlaying 3D distribution onto molecular networking provided further insights into functional interconnections in molecular distributions, not accessible otherwise. For example, the association with HLB symptoms is notably different for oxidized versions of some flavonoids. As shown in Fig. 2, hesperidin accumulation mirrored declines in the flavonoid didymin, possibly reflecting oxidative conversion of the latter into the former during infection. Such localized oxidative shifts were further evident across flavonoid families (Fig. S3), aligning with oxidative stress reports previously described[41,42]. In another example, 3D maps revealed that leaf age was the predominant driver of flavonoid abundance, rather than disease severity. Younger leaves possess elevated flavonoids, necessitating age-matching to correctly determine infection biomarkers.

Exploring the HLB-discriminating ability and corresponding 3D maps for various metabolites allowed us to identify other molecules of interest in addition to flavonoids. In particular, feruloylputrescine was noted to be highly associated with symptom severity. Distribution patterns implicated the conversion of ferulic acid into feruloylputrescine, mirrored by ferulate disappearance and putrescine buildup (Fig. 3). This shift was further echoed by hydroxycinnamate rises, likely reflecting the oxidation of cinnamic acid precursors. Taken together, spatial patterns indicate metabolic channeling away from phenylpropanoid biosynthesis toward polyamine conjugation due to infection.

Exploring upstream pathways points to a branch point: while general phenylalanine supply appeared unaffected, p-coumaroyl-CoA intermediates depleting from the flavonoid pathway were instead visible as

hydroxycinnamate en route to feruloylputrescine. This suggests that *C*Las has evolved to counteract both ferulic acid and flavonoids formation, ostensibly as a self-defense against their toxicity.

To confirm that these molecules are indeed toxic to *C*Las, we conducted the disc and hairy roots assays that confirmed their bactericidal effects toward *C*Las. Although the disc assay exploited a surrogate organism, *Liberibacter crescens,* the hairy roots assay is a way to directly assess the toxicity, both genetic- and chemical-based to *C*Las itself[35,43,44]. In this approach, *C*Las is maintained in citrus hairy root tissues, and the antimicrobials are directly infiltrated into the roots by vacuum, thus overcoming the delivery bottleneck that exists with conventional whole tree assays[13,36,45]. Additionally, because citrus hairy roots have intact vasculature, they are much closer to the *in planta* citrus environment where *C*Las resides, thus providing reliability over testing against surrogate bacteria or heterologous systems[46–49]. The assay has demonstrated a clear bactericidal effect of the flavonoids on par with the anti-*C*Las activity of oxytetracycline. In the case of ferulic acid, the lower dosages (125 to 250 ppm) are highly effective, while increasing the dosage to 500 or 1000 ppm did not seem to be effective, possibly due to the toxicity of the compounds to the hairy roots themselves[50]. Both flavonoids and ferulic acid bacterial inhibitory abilities have been well characterized in other systems, but the mode of action is not clear[51,52]. These phytochemicals may disrupt bacterial cell-to-cell communication[53], modify biofilm production and inhibit swimming motility[54], impact bacterial membranes[55], or even create pores or rupture cell members[56]. Nevertheless, these experiments confirmed the robust anti-*C*Las activity of the flavonoids[55,56]. It is not known how these compounds may impact other members of the citrus microbiome. Indeed, both bacterial and fungi communities drastically shift as HLB symptoms advance[9], and citrus-associated fungi can produce *Liberibacter* spp. inhibitor compounds[34]. Future studies should consider the interactions of these compounds with the microbiome, and vice versa, to increase efficacy of disease management applications.

With the efficacy against *C*Las confirmed, the ferulic acid and bioflavonoids present an opportunity for field application as novel Huanglongbing therapies. These compounds are plant-derived, non-toxic, biodegradable, inexpensive to manufacture at scale, and thus would be a very appealing class of therapeutics. They may help to bypass negative environmental and economic externalities compared to current methods, such as antibiotic use and synthetic chemical pesticide applications for ACP control[12–15]. While optimal therapy delivery systems for citrus plants remain an active topic of research and development, multiple practical options such as trunk injection already exist[9,13,14,37,57–60].

The impact of HLB has been devastating. Deployed alongside psyllid population suppression, the proposed "botanical" solutions harnessing natural plant defenses, when deployed at scale, may offer a viable path towards stable HLB mitigation and control. Finally, although we demonstrate the described approach for the citrus and *C*Las, the same approach of mapping the metabolic distributions coupled with toxicity assays may present opportunities to generalize the development of a therapy agent discovery pipeline that could be used for a wide range of pathosystems.

Materials and methods

Tissue collection and processing

Branch and single leaf assay

For the branch and single leaf assays, Valencia sweet orange (*Citrus sinensis*) grafted onto Swingle rootstock was propagated in a greenhouse and inoculated with *C*Las using infectious ACP. Five ACP adults enclosed in a nylon mesh drawstring bag were applied and confined to newly emerged leaves for 14 days. Trees were then treated with insecticides, imidacloprid, and carbaryl, to eliminate ACP, and the trees were kept free of ACP until the time of sampling. For branch analyses, all leaves for a given time point were detached via razor blades, flash-frozen, and held in liquid nitrogen during sampling. Petioles were removed and stored at − 80 °C for *C*Las quantitation via qPCR. For metabolome analysis, 1/8 in (3.175 mm) diameter punches were dispensed into the wells of 96 well plates containing 500 µL 50% ethanol. Tissues were lysed by repeat freeze–thaw cycles between − 80 °C and room temperature. The resulting extracts were filtered through 0.22 um filter plates via centrifugation before analysis via LC–MS. Leaf punches were collected in the same manner for the single-leaf assay.

Field collected tissues

Stems, roots, and leaves from 50 trees (n = 150) were collected from 5 different citrus Florida citrus groves in 2016[9]. In 2017, stems, roots, and leaves were collected from 80 trees located in 7 different orchards (n = 240). The stem collection included both xylem and phloem.

Each tree was divided into 4 quadrants (North, South, East, and West), and stems with attached leaves were collected from each of the quadrants and pooled. Topsoil from two sides of the tree and approximately 1.5 feet away from the base of the trunk near the irrigation line was removed, and the feeder roots near the irrigation line were sampled, shaken to remove soil, and sealed in a plastic bag. Gloves were changed, and clippers and shovels were sterilized with 30% household bleach between each tree that was sampled. All samples were immediately placed on ice for transit to the laboratory, where they were placed at 4˚C and processed within 24 h.

MS data acquisition

The tissue extracts were prepared in 100% ethanol, spiked with 1 µM sulfadimethoxine internal standard, and analyzed with UltiMate 3000 UPLC system (Thermo Scientific) using a Kinetex™ 1.7 µm C18 reversed-phase UHPLC column (50 X 2.1 mm) and Maxis Q-TOF mass spectrometer (Bruker Daltonics) equipped with ESI source. The column was equilibrated with 2% solvent B (98% acetonitrile, 0.1% formic acid in LC–MS grade water with solvent A as 0.1% formic acid in water), followed by a linear gradient from 2 B to 10% B in 0.2 min and then to 100% B at 12 min, held at 100% B for 2 min. Following each run, the column was equilibrated at 2% B for 1 min at a flow rate of 0.5 mL/min. MS spectra were acquired in positive ion mode in the range of 80–2000 m/z.

A mixture of 10 µg/mL of each sulfamethazine, sulfamethizole, sulfachloropyridazine sulfadimethoxine, amitriptyline, and coumarin-314 was run at the beginning and the end of each batch (one 96-well plate). An external calibration with ESI-L Low Concentration Tuning Mix (Agilent Technologies) was performed prior to data collection, and internal calibrant Hexakis(1H,1H,3H-tertrafluoropropoxy)phosphazene was used throughout the runs. The capillary voltage of 4500 V, nebulizer gas pressure (nitrogen) of 1.4 bar, ion source temperature of 180 °C, and dry gas flow of 4 L/min, were used. For acquiring MS/MS fragmentation, the 7 most intense ions per MS[1] were selected. A stepping function was used to fragment ions at 50%, 100%, 150%, and 200% of the CID, with a timing of 25% for each step. Similarly, basic stepping of collision RF of 250 to 1500 Vpp with a timing of 25% for each step and transfer time stepping of 50, 75, 100, and 150 µs with a timing of 25% for each step was employed. MS/MS active exclusion parameter was set to 5 and released after 30 s. The mass of internal calibrant was excluded from the MS/MS list using a mass range of *m/z* 921.5–924.5. The data were deposited in the MassIVE online repository and are available under the IDs: MSV000082967 (2D leaf mapping); MSV000082962 (3D branch mapping); MSV000082963 and MSV000085416 (field study).

MS data analysis

The collected HPLC–MS raw data files were first converted from Bruker's *d* to mzXML format and then processed with the open-source MZmine2 software [https://www.ncbi.nlm.nih.gov/pubmed/20650010?dopt=Abstract]. crop filtering with a retention time (RT) range of 0 to 14 min chromatograms. Mass detection was performed with a signal threshold of 1E3 and a 0.04-s minimum peak width. The mass tolerance was set to 20 ppm, and the maximum allowed retention time deviation was set to 5 s. For chromatographic deconvolution, the local minimum search algorithm with a 30% chromatographic threshold, minimum RT range of 0.6 s, minimum relative height of 1%, minimum absolute height of 5E2, the minimum ratio of peak top/edge 2, and peak duration range of 0.04—min was used. After isotope peak removal, the peak lists of all samples were aligned within the corresponding retention time and mass tolerances. Gap filling was performed on the aligned peak list using the peak finder module with 1% intensity, 10-ppm *m/z* tolerance, and 0.05-min RT tolerance, respectively. After the creation and export of a feature matrix containing the feature retention times, exact mass, and peak areas of the corresponding extracted ion chromatograms, the sample metadata was added to the feature matrix metadata of the samples.

All of the peaks that were present in any of the blanks with a signal-to-noise ratio (S/N) below 3:1 were removed from the final feature table.

Data pretreatment and statistical analysis

The data pretreatment and following statistical analysis were carried out with the MetaboAnalyst platform[61]. The feature tables generated with MZmine were filtered to remove features with near-constant, very small values and values with low repeatability using the interquartile range (IQR) estimate. A detailed description of the methodology is given in Ref.[62]. The samples were normalized using quantile normalization. The data were further scaled by mean centering and divided by standard deviation for each feature.

Principal component analysis (PCA) and partial least-squares discriminant analysis (PLS-DA)[63] were used to explore and visualize variance within data and differences among experimental categories. Random forests (RF)[64] supervised analysis was used to further verify the validity of determined discriminating features.

Molecular networking

The molecular network was created using the online workflow at GNPS platform (gnps.ucsd.edu)[25,26]. The data were clustered with MS-Cluster with a parent mass tolerance of 0.1 Da and an MS/MS fragment ion tolerance of 0.1 Da to create consensus spectra. The consensus spectra that contained less than 3 spectra were discarded. A network was then created where edges were filtered to have a cosine score above 0.65 and more than 4 matched peaks. The edges between two nodes were kept in the network if and only if each of the nodes appeared in each other's respective top 10 most similar nodes. The spectra in the network were then searched against GNPS's spectral libraries. All matches kept between network spectra and library spectra were required to have a score above 0.7 and at least 5 matched peaks. The molecular networks and the parameters used are available at the links below: 2D leaf mapping: https://gnps.ucsd.edu/ProteoSAFe/status.jsp?task=105598d2d782412ca0c988bfe933c032, 3D branch mapping: https://gnps.ucsd.edu/ProteoSAFe/status.jsp?task=e2f1a1e367a7450fb940fe7cda04dc19, Field study: https://gnps.ucsd.edu/ProteoSAFe/status.jsp?task=2b0b1e554bc14d1fba321257b0ffc827, Field study, feature-based molecular network[65]: https://gnps.ucsd.edu/ProteoSAFe/status.jsp?task=4ac8aff08af5433292143047c8cc5e90.

2D/3D visualization

The procedure for the creation and visualization of 3D models is described in detail previously[21]. Briefly, the 2D images and 3D model of the sampled plants were created and the coordinates for sampled spots were selected according to described protocol[21]. The abundances of detected metabolites were normalized and autoscaled[61], and the coordinates for spots corresponding to each sample were inserted into the feature tables along with the spot size. The 2D or 3D models were drag-and-dropped into the 'ili website in the browser (https://ili.embl.de/), followed by the feature table with coordinates. All figures were generated with the "Jet" color map. Spot size, opacity, and border opacity were adjusted for optimal visualization.

Synthesis of feruloyl putrescine hydrochloride

As the feruloyl putrescine was not available commercially, we have synthesized this compound for further compound identification validation and disc assay testing. *N*-Boc putrescine (1 equiv, 4.25 mmol, 0.91 mL) and ferulic

acid (1.06 equiv, 4.5 mmol, 880 mg) were combined in anhydrous CH_2Cl_2 (32.5 mL) with stirring and the solution was cooled to 0 °C. Then, a solution of N,N′-dicyclohexylcarbodiimide (DCC, 1.7 equiv, 7.2 mmol, 1.49 g) in anhydrous CH_2Cl_2 was added dropwise. The reaction mixture was allowed to warm to room temperature and stirred at rt for 2 days. Then, the mixture was filtered to remove precipitated dicyclohexylurea and the filtrate was concentrated *in vacuo*. The crude residue was purified over silica gel using 2–4% MeOH in CH_2Cl_2 to afford *N*-Boc feruloyl putrescine as a light yellow solid in 78% yield (1.29 g). For Boc deprotection, trifluoroacetic acid (TFA, 15 mL) was added to a stirred solution of *N*-Boc feruloyl putrescine in CH_2Cl_2 (75 mL) under an inert atmosphere of Ar. The reaction was allowed to stir at room temperature for 40 min, then the solvent was removed *in vacuo.* The residue was dissolved in methanol (15 mL) with HCl (25 mL) and evaporated *in vacuo* to yield feruloyl putrescine hydrochloride as a light yellow solid (75% overall yield). ^{1}H and ^{13}C NMR data were consistent with those previously reported[66]. HRMS (ESI) exact mass calculated for $[M+H]^+$ ($C_{14}H_{21}N_2O_3$) is m/z 265.1547.

Simulations

Simulations were performed using the *C*Las Ishi-1 M15 metabolic model[15]. Standard biomass constraints were maintained to predict the overall *C*Las growth rate. All model simulations were performed using the Gurobi Optimizer v.5.6.3 solver (Gurobi Optimization) in the COBRA toolbox[67] for MATLAB (MathWorks). We simulated the maximal growth rate of *C*Las using flux-balance analysis. The main metabolic compounds affecting *C*Las growth were identified using the metabolome data, that was anthranilate, ferulate, glutamate, N-acetyl-L-ornithine, ornithine, putrescine, tyrosine, and vanillin and sensitivity analysis, looking for metabolite-specific growth responses was performed by varying uptake rates among 1×10^{-12}, 1×10^{-10}, 1×10^{-8}, 1×10^{-6}, 1×10^{-4}, 1×10^{-2}, 1×10^{-1}, 1×10^{0}, 1×10^{1}, 1×10^{2}, 1×10^{3}. Additionally, we performed a sensitivity analysis, which deployed a phenotypic phase plane that facilitates the observation of effects on the *C*Las growth by varying a particular constraint, in this case putrescine and ferulic acid. Predicted growth rates were compared with experimental results.

Microbial culture assays

Citrus metabolites were assayed using a previously developed disc-diffusion assay for *L. crescens*[34]. Briefly, *L. crescens* liquid cultures were incorporated to a soft agar (0.8%) overlay and applied to a 20 mL solid agar (1.5%). *L. crescens* strain BT-1] was maintained and grown exclusively on the previously described bBM7 + 1.0 methyl-β-cyclodextrin. To these overlaid plates were applied autoclave-sterilized 6 mm paper discs (Whatman, NJ, USA), previously loaded with 35 µL of a given metabolite solution and dried in a sterile biosafety cabinet. Once discs were applied, plates were sealed and stored upside down in a 28 ℃ incubator for 6 days to allow a clear zone of inhibition development for measurement. 35 mg/mL solutions of putrescine (Fisher Scientific, Waltham, MA, USA), and feruloylputrescine (synthesis described above) were prepared using sterile water.

The efficacy of bioflavonoids and ferulic acid in vitro *C*Las-hairy root assay

The in vitro *C*Las-hairy roots assay was performed according to the previously described protocol[35]. *C*Las-citrus hairy roots were generated using *C*Las-infected citrus plant tissues, and the diagnosis of *C*Las was confirmed by quantitative PCR (qPCR). *C*Las-hairy roots were surface sterilized, and ~ 100 mg was transferred into multi-well plates containing Gamborg's B-5 medium with 1% sucrose. Different concentrations of bioflavonoids (Horbaach, https://horbaach.com/products/citrus-bioflavonoids-complex-1500mg-300-vegetarian-caplets) and ferulic acid (Fisher Scientific, Pittsburgh, PA, Catalog No. ICN10168505): 125, 250, 500, and 1000 ppm/mL, were added, vacuum infiltrated and incubated on a rotator shaker at 50 rpm in the dark at 25 °C for 72 h. The experiments were carried out with six biological replicates, positive control of oxytetracycline hydrochloride (Sigma Aldrich, Burlington, MA), untreated *C*Las hairy roots, and an equal concentration of ethanol solvent used to dissolve the bioflavonoids and ferulic acid as negative controls. After the treatments, tissue samples were treated with PMAxx dye (propidium monoazide, Biotium, Fremont, CA) to inactivate dead *C*Las bacterial DNA. Further, total DNA was extracted, and viable bacterial titer was estimated by qPCR analysis using primers specific to the *C*Las gene encoding the Ribonucleotide reductase β-subunit (nrdB, RNR-F/RNR-R)[68] and the relative *C*Las titers were estimated and plotted relative to untreated using the $2-\Delta\Delta Ct$ method. After normalization of target Ct with an endogenous reference gene (Ct') glyceraldehyde3-phosphate dehydrogenase 2 (GAPC2)[69] to correct for DNA template concentration differences among the samples, it was plotted relative to untreated controls.

Primers used in this study

RNR-F	CATGCTCCATGAAGCTACCC	[68]
RNR-R	GGAGCATTTAACCCCACGAA	
GAPC2-F	GAGGAGATCCCATGGGCAAA	[69]
GAPC2-R	AAGAGGAGCTAGGCAGTTGG	

Data availability

The data were deposited in the MassIVE online repository and are available below links: https://massive.ucsd.edu/ProteoSAFe/dataset.jsp?task=bc1261c22e6c49d1b4f6490c7414845b, https://massive.ucsd.edu/ProteoSAFe/dataset.jsp?task=2008873282ac4beda2a008ada2917fa4, https://massive.ucsd.edu/ProteoSAFe/dataset.jsp?task=d4416036d13141b9b3008c7712395534, https://massive.ucsd.edu/ProteoSAFe/dataset.jsp?task=7db2bd0c5a0941f28286cabdc407a17f, https://massive.ucsd.edu/ProteoSAFe/dataset.jsp?task=25598a865760458fbc45a3f579c8479c.

Received: 5 April 2024; Accepted: 16 August 2024
Published online: 02 September 2024

References

1. Liu, Y., Heying, E. & Tanumihardjo, S. A. History, global distribution, and nutritional importance of citrus fruits. *Compr. Rev. Food Sci. Food Saf.* **11**, 530–545 (2012).
2. Alvarez, S., Rohrig, E., Solís, D. & Thomas, M. H. Citrus greening disease (Huanglongbing) in Florida: Economic impact, management and the potential for biological control. *Agric. Res.* **5**, 109–118 (2016).
3. Bové, J. M. Huanglongbing: A destructive, newly-emerging, century-old disease of citrus. *J. Plant Pathol.* **88**, 7–37 (2006).
4. Lee, J. A. *et al.* Asymptomatic spread of Huanglongbing and implications for disease control. *Proc. Natl. Acad. Sci. U. S. A.* **112**, 7605–7610 (2015).
5. Manjunath, K. L., Halbert, S. E., Ramadugu, C., Webb, S. & Lee, R. F. Detection of 'Candidatus *Liberibacter asiaticus*' in *Diaphorina citri* and its importance in the management of citrus Huanglongbing in Florida. *Phytopathology®* **98**, 387–396 (2008).
6. Gottwald, T. R. Current epidemiological understanding of citrus Huanglongbing. *Annu. Rev. Phytopathol.* **48**, 119–139 (2010).
7. Boina, D. R. & Bloomquist, J. R. Chemical control of the Asian citrus psyllid and of Huanglongbing disease in citrus. *Pest Manag. Sci.* **71**, 808–823 (2015).
8. Ghosh, D. *et al.* Huanglongbing pandemic: Current challenges and emerging management strategies. *Plants* **12**, 160 (2022).
9. Ginnan, N. A. *et al.* Disease-induced microbial shifts in citrus indicate microbiome-derived responses to Huanglongbing across the disease severity spectrum. *Phytobiomes J.* **4**, 375–387 (2020).
10. Zhong, Y. *et al.* Comparative transcriptome and iTRAQ proteome analyses of citrus root responses to Candidatus *Liberibacter asiaticus* infection. *PLoS One* **10**, e0126973 (2015).
11. Li, B., Zhang, Y., Qiu, D., Francis, F. & Wang, S. Comparative proteomic analysis of sweet orange petiole provides insights into the development of Huanglongbing symptoms. *Front. Plant Sci.* **12**, 656997 (2021).
12. Yang, C. *et al.* Metagenomic analysis reveals the mechanism for the observed increase in antibacterial activity of penicillin against uncultured bacteria *Liberibacter asiaticus* relative to oxytetracycline in planta. *Antibiotics (Basel)* **9**, 874 (2020).
13. Zhang, M. *et al.* Effective antibiotics against 'Candidatus *Liberibacter asiaticus*' in HLB-affected citrus plants identified via the graft-based evaluation. *PLoS One* **9**, e111032 (2014).
14. Hu, J. & Wang, N. Evaluation of the spatiotemporal dynamics of oxytetracycline and its control effect against citrus Huanglongbing via trunk injection. *Phytopathology* **106**, 1495–1503 (2016).
15. Zuñiga, C. *et al.* Linking metabolic phenotypes to pathogenic traits among 'Candidatus *Liberibacter asiaticus*' and its hosts. *NPJ Syst. Biol. Appl.* **6**, 24 (2020).
16. Schauer, N. & Fernie, A. R. Plant metabolomics: Towards biological function and mechanism. *Trends Plant Sci.* **11**, 508–516 (2006).
17. Macel, M., Van Dam, N. M. & Keurentjes, J. J. B. Metabolomics: The chemistry between ecology and genetics. *Mol. Ecol. Resour.* **10**, 583–593 (2010).
18. Yao, L. *et al.* Proteomic and metabolomic analyses provide insight into the off-flavour of fruits from citrus trees infected with 'Candidatus *Liberibacter asiaticus*'. *Hortic. Res.* **6**, 31 (2019).
19. Hijaz, F. M. *et al.* An HPLC-MS characterization of the changes in sweet orange leaf metabolite profile following infection by the bacterial pathogen Candidatus *Liberibacter asiaticus*. *PLoS One* **8**, e79485 (2013).
20. Aksenov, A. A. *et al.* Detection of Huanglongbing disease using differential mobility spectrometry. *Anal. Chem.* **86**, 2481–2488 (2014).
21. Protsyuk, I. *et al.* 3D molecular cartography using LC-MS facilitated by Optimus and 'ili software. *Nat. Protoc.* **13**, 134–154 (2018).
22. Kapono, C. A. *et al.* Creating a 3D microbial and chemical snapshot of a human habitat. *Sci. Rep.* **8**, 3669 (2018).
23. Floros, D. J. *et al.* Mass spectrometry based molecular 3D-cartography of plant metabolites. *Front. Plant Sci.* **8**, 429 (2017).
24. Bouslimani, A. *et al.* Molecular cartography of the human skin surface in 3D. *Proc. Natl. Acad. Sci. U. S. A.* **112**, E2120–E2129 (2015).
25. Wang, M. *et al.* Sharing and community curation of mass spectrometry data with global natural products social molecular networking. *Nat. Biotechnol.* **34**, 828–837 (2016).
26. Aron, A. T. *et al.* Reproducible molecular networking of untargeted mass spectrometry data using GNPS. *Nat. Protoc.* https://doi.org/10.1038/s41596-020-0317-5 (2020).
27. Watrous, J. *et al.* Mass spectral molecular networking of living microbial colonies. *Proc. Natl. Acad. Sci. U. S. A.* **109**, E1743–E1752 (2012).
28. KEGG PATHWAY: Phenylpropanoid biosynthesis - Citrus sinensis (Valencia orange). https://www.genome.jp/kegg-bin/show_pathway?cit00940.
29. Feng, G., Ai, X., Yi, H., Guo, W. & Wu, J. Genomic and transcriptomic analyses of *Citrus sinensis* varieties provide insights into Valencia orange fruit mastication trait formation. *Hortic. Res.* **8**, 218 (2021).
30. Chen, Q. *et al.* Metabolomic analysis revealed distinct physiological responses of leaves and roots to Huanglongbing in a citrus rootstock. *Int. J. Mol. Sci.* **23**, 9242 (2022).
31. Chin, E. L., Mishchuk, D. O., Breksa, A. P. & Slupsky, C. M. Metabolite signature of Candidatus *Liberibacter asiaticus* infection in two citrus varieties. *J. Agric. Food Chem.* **62**, 6585–6591 (2014).
32. Deng, H. *et al.* Comparative leaf volatile profiles of two contrasting mandarin cultivars against *Liberibacter asiaticus* infection illustrate Huanglongbing tolerance mechanisms. *J. Agric. Food Chem.* **69**, 10869–10884 (2021).
33. Padhi, E. M. T. *et al.* Metabolome and microbiome signatures in the roots of citrus affected by Huanglongbing. *Phytopathology* **109**, 2022–2032 (2019).
34. Blacutt, A. *et al.* An in vitro pipeline for screening and selection of citrus-associated microbiota with potential anti-'Candidatus *Liberibacter asiaticus*' properties. *Appl. Environ. Microbiol.* https://doi.org/10.1128/AEM.02883-19 (2020).
35. Irigoyen, S. *et al.* Plant hairy roots enable high throughput identification of antimicrobials against *Candidatus Liberibacter* spp. *Nat. Commun.* **11**, 5802 (2020).
36. Li, J. *et al.* The in planta effective concentration of oxytetracycline against ' *Liberibacter asiaticus*' for suppression of citrus Huanglongbing. *Phytopathology* **109**, 2046–2054 (2019).
37. Hu, J., Jiang, J. & Wang, N. Control of CITRUS Huanglongbing via trunk injection of plant defense activators and antibiotics. *Phytopathology* **108**, 186–195 (2018).
38. Munir, S. *et al.* Unraveling the metabolite signature of citrus showing defense response towards Candidatus *Liberibacter asiaticus* after application of endophyte *Bacillus subtilis* L1–21. *Microbiol. Res.* **234**, 126425 (2020).
39. Hung, W.-L. & Wang, Y. A targeted mass spectrometry-based metabolomics approach toward the understanding of host responses to Huanglongbing disease. *J. Agric. Food Chem.* **66**, 10651–10661 (2018).
40. Suh, J. H., Tang, X., Zhang, Y., Gmitter, F. G. Jr. & Wang, Y. Metabolomic analysis provides new insight into tolerance of Huanglongbing in Citrus. *Front. Plant Sci.* **12**, 710598 (2021).
41. Nuutila, A. M., Kammiovirta, K. & Oksman-Caldentey, K.-M. Comparison of methods for the hydrolysis of flavonoids and phenolic acids from onion and spinach for HPLC analysis. *Food Chem.* **76**, 519–525. https://doi.org/10.1016/s0308-8146(01)00305-3 (2002).

42. Pourcel, L., Routaboul, J., Cheynier, V., Lepiniec, L. & Debeaujon, I. Flavonoid oxidation in plants: from biochemical properties to physiological functions. *Trends Plant Sci.* **12**, 29–36. https://doi.org/10.1016/j.tplants.2006.11.006 (2007).
43. Mandadi, K. *et al.* Hairy roots to the rescue: Speeding up discovery for HLB Management. *Citrograph* **11**, 20–22 (2020).
44. Kennedy, J. P. *et al.* A perspective on current therapeutic molecule screening methods against ' *Liberibacter asiaticus*', the presumed causative agent of citrus Huanglongbing. *Phytopathology* **113**, 1171–1179 (2023).
45. Zhang, M. *et al.* Field evaluation of integrated management for mitigating citrus Huanglongbing in Florida. *Front. Plant Sci.* **9**, 1890 (2018).
46. Davis, M. J., Mondal, S. N., Chen, H., Rogers, M. E. & Brlansky, R. H. Co-cultivation of 'Candidatus *Liberibacter asiaticus*' with actinobacteria from citrus with Huanglongbing. *Plant Dis.* **92**, 1547–1550 (2008).
47. Leonard, M. T., Fagen, J. R., Davis-Richardson, A. G., Davis, M. J. & Triplett, E. W. Complete genome sequence of *Liberibacter crescens* BT-1. *Stand. Genom. Sci.* **7**, 271–283 (2012).
48. Barnett, M. J., Solow-Cordero, D. E. & Long, S. R. A high-throughput system to identify inhibitors of *Liberibacter asiaticus* transcription regulators. *Proc. Natl. Acad. Sci. U. S. A.* **116**, 18009–18014 (2019).
49. Jain, M. *et al.* Is a cultured surrogate for functional genomics of uncultured pathogenic 'Liberibacter' spp. and is naturally competent for transformation. *Phytopathology* **109**, 1811–1819 (2019).
50. dos Santos, W. D. *et al.* Soybean (Glycine max) root lignification induced by ferulic acid. The possible mode of action. *J. Chem. Ecol.* **34**, 1230–1241 (2008).
51. Cushnie, T. P. T. & Lamb, A. J. Antimicrobial activity of flavonoids. *Int. J. Antimicrob. Agents* **26**, 343–356 (2005).
52. Ou, S. & Kwok, K.-C. Ferulic acid: Pharmaceutical functions, preparation and applications in foods. *J. Sci. Food Agric.* **84**, 1261–1269 (2004).
53. Paczkowski, J. E. *et al.* Flavonoids suppress virulence through allosteric inhibition of quorum-sensing receptors. *J. Biol. Chem.* **292**, 4064–4076 (2017).
54. Borges, A., Saavedra, M. J. & Simões, M. The activity of ferulic and gallic acids in biofilm prevention and control of pathogenic bacteria. *Biofouling* **28**, 755–767 (2012).
55. Li, A.-P., He, Y.-H., Zhang, S.-Y. & Shi, Y.-P. Antibacterial activity and action mechanism of flavonoids against phytopathogenic bacteria. *Pestic. Biochem. Physiol.* **188**, 105221 (2022).
56. Borges, A., Ferreira, C., Saavedra, M. J. & Simões, M. Antibacterial activity and mode of action of ferulic and gallic acids against pathogenic bacteria. *Microb. Drug Resist.* **19**, 256–265 (2013).
57. Archer, L., Kunwar, S., Alferez, F., Batuman, O. & Albrecht, U. Trunk injection of oxytetracycline for Huanglongbing management in mature grapefruit and sweet orange trees. *Phytopathology* **113**, 1010–1021 (2023).
58. Blaustein, R. A., Lorca, G. L. & Teplitski, M. Challenges for managing *Candidatus Liberibacter* spp. (Huanglongbing disease pathogen): Current control measures and future directions. *Phytopathology* **108**, 424–435 (2018).
59. Gardner, C. L. *et al.* Assessment of unconventional antimicrobial compounds for the control of 'Candidatus *Liberibacter asiaticus*', the causative agent of citrus greening disease. *Sci. Rep.* **10**, 5395 (2020).
60. Archer, L., Qureshi, J. & Albrecht, U. Efficacy of trunk injected imidacloprid and oxytetracycline in managing huanglongbing and Asian citrus psyllid in infected sweet orange (*Citrus sinensis*) trees. *Collect. FAO Agric.* **12**, 1592 (2022).
61. Xia, J. & Wishart, D. S. Using MetaboAnalyst 3.0 for comprehensive metabolomics data analysis. *Curr. Protoc. Bioinform.* **55**, 14.10.1-14.10.91 (2016).
62. Hackstadt, A. J. & Hess, A. M. Filtering for increased power for microarray data analysis. *BMC Bioinform.* https://doi.org/10.1186/1471-2105-10-11 (2009).
63. Wold, S., Sjöström, M. & Eriksson, L. PLS-regression: A basic tool of chemometrics. *Chemom. Intell. Lab. Syst.* **58**, 109–130 (2001).
64. Breiman, L. Random forests. *Mach. Learn.* **45**, 5–32 (2001).
65. Nothias, L. F. *et al.* Feature-based molecular networking in the GNPS analysis environment. *Nat. Methods* https://doi.org/10.1101/812404 (2019).
66. Kyselka, J. *et al.* Antifungal polyamides of hydroxycinnamic acids from sunflower bee pollen. *J. Agric. Food Chem.* **66**, 11018–11026. https://doi.org/10.1021/acs.jafc.8b03976 (2018).
67. Schellenberger, J. *et al.* Quantitative prediction of cellular metabolism with constraint-based models: The COBRA Toolbox v2.0. *Nat. Protoc.* **6**, 1290–1307 (2011).
68. Zheng, Z. *et al.* Unusual five copies and dual forms of nrdB in 'Candidatus *Liberibacter asiaticus*': Biological implications and PCR detection application. *Sci. Rep.* **6**, 39020 (2016).
69. Mafra, V. *et al.* Reference genes for accurate transcript normalization in citrus genotypes under different experimental conditions. *PLoS One* **7**, e31263 (2012).

Acknowledgements

This work was partly supported by USDA NIFA grant no. 2017-70016-26053; USDA NIFA grants 2021-70029-36056, and Texas A&M AgriLife Insect-vector disease seed grants to K.M. AAA, AL were supported by the USDA NIFA GRANT 13665683. The Authors are grateful to Dr. Greg McCollum.

Author contributions

CR, PR, PCD created the idea for the work. NG, AB, GM, PR collected plant tissues NG, AB extracted plant tissues for acquisition of mass spectrometry data AA acquired mass spectrometry data AA, AM analyzed mass spectrometry data GM conducted plants growth, infection by CLas, PCR diagnostics AM created 3D models AB, AM picked coordinates on plant models AA performed statistical analysis EG performed organic synthesis CZ, KZ performed and analyzed model simulations AB performed disk assays MR, KM conducted hairy roots assay AA wrote the manuscript CR, AB, PR, NG, AL edited the manuscript.

Competing interests

AAA and AVM are founders of Arome Science, Inc. PCD is an advisor of and holds equity in Cybele, consulted for MSD Animal Health in 2023 and is a cofounder of, holds equity in and is scientific advisor for Ometa Labs, Arome and Enveda with prior approval by the University of California San Diego. The remaining authors declare no competing interests.

Additional information

Supplementary Information The online version contains supplementary material available at https://doi.org/10.1038/s41598-024-70499-z.

Correspondence and requests for materials should be addressed to A.A.A.

Terms and Conditions

Springer Nature journal content, brought to you courtesy of Springer Nature Customer Service Center GmbH (“Springer Nature”).
Springer Nature supports a reasonable amount of sharing of research papers by authors, subscribers and authorised users (“Users”), for small-scale personal, non-commercial use provided that all copyright, trade and service marks and other proprietary notices are maintained. By accessing, sharing, receiving or otherwise using the Springer Nature journal content you agree to these terms of use (“Terms”). For these purposes, Springer Nature considers academic use (by researchers and students) to be non-commercial.
These Terms are supplementary and will apply in addition to any applicable website terms and conditions, a relevant site licence or a personal subscription. These Terms will prevail over any conflict or ambiguity with regards to the relevant terms, a site licence or a personal subscription (to the extent of the conflict or ambiguity only). For Creative Commons-licensed articles, the terms of the Creative Commons license used will apply.
We collect and use personal data to provide access to the Springer Nature journal content. We may also use these personal data internally within ResearchGate and Springer Nature and as agreed share it, in an anonymised way, for purposes of tracking, analysis and reporting. We will not otherwise disclose your personal data outside the ResearchGate or the Springer Nature group of companies unless we have your permission as detailed in the Privacy Policy.
While Users may use the Springer Nature journal content for small scale, personal non-commercial use, it is important to note that Users may not:

1. use such content for the purpose of providing other users with access on a regular or large scale basis or as a means to circumvent access control;
2. use such content where to do so would be considered a criminal or statutory offence in any jurisdiction, or gives rise to civil liability, or is otherwise unlawful;
3. falsely or misleadingly imply or suggest endorsement, approval , sponsorship, or association unless explicitly agreed to by Springer Nature in writing;
4. use bots or other automated methods to access the content or redirect messages
5. override any security feature or exclusionary protocol; or
6. share the content in order to create substitute for Springer Nature products or services or a systematic database of Springer Nature journal content.

In line with the restriction against commercial use, Springer Nature does not permit the creation of a product or service that creates revenue, royalties, rent or income from our content or its inclusion as part of a paid for service or for other commercial gain. Springer Nature journal content cannot be used for inter-library loans and librarians may not upload Springer Nature journal content on a large scale into their, or any other, institutional repository.
These terms of use are reviewed regularly and may be amended at any time. Springer Nature is not obligated to publish any information or content on this website and may remove it or features or functionality at our sole discretion, at any time with or without notice. Springer Nature may revoke this licence to you at any time and remove access to any copies of the Springer Nature journal content which have been saved.
To the fullest extent permitted by law, Springer Nature makes no warranties, representations or guarantees to Users, either express or implied with respect to the Springer nature journal content and all parties disclaim and waive any implied warranties or warranties imposed by law, including merchantability or fitness for any particular purpose.
Please note that these rights do not automatically extend to content, data or other material published by Springer Nature that may be licensed from third parties.
If you would like to use or distribute our Springer Nature journal content to a wider audience or on a regular basis or in any other manner not expressly permitted by these Terms, please contact Springer Nature at

onlineservice@springernature.com